







BRIEF DEFINITIVE REPORT

Homozygous *STAT2* gain-of-function mutation by loss of *USP18* activity in a patient with type I interferonopathy

Conor Gruber¹, Marta Martin-Fernandez¹ , Fatima Ailal^{2,3} , Xueer Qiu¹, Justin Taft¹, Jennie Altman¹, Jérémie Rosain^{4,5}, Sofija Buta¹ , Aziz Bousfiha^{2,3} , Jean-Laurent Casanova^{4,5,6,7,8} , Jacinta Bustamante^{4,5,6,9}, and Dusan Bogunovic^{1,10,11,12} 

Type I interferonopathies are monogenic disorders characterized by enhanced type I interferon (IFN-I) cytokine activity. Inherited *USP18* and *ISG15* deficiencies underlie type I interferonopathies by preventing the regulation of late responses to IFN-I. Specifically, *USP18*, being stabilized by *ISG15*, sterically hinders *JAK1* from binding to the *IFNAR2* subunit of the IFN-I receptor. We report an infant who died of autoinflammation due to a homozygous missense mutation (R148Q) in *STAT2*. The variant is a gain of function (GOF) for induction of the late, but not early, response to IFN-I. Surprisingly, the mutation does not enhance the intrinsic activity of the *STAT2*-containing transcriptional complex responsible for IFN-I-stimulated gene induction. Rather, the *STAT2* R148Q variant is a GOF because it fails to appropriately traffic *USP18* to *IFNAR2*, thereby preventing *USP18* from negatively regulating responses to IFN-I. Homozygosity for *STAT2* R148Q represents a novel molecular and clinical phenocopy of inherited *USP18* deficiency, which, together with inherited *ISG15* deficiency, defines a group of type I interferonopathies characterized by an impaired regulation of late cellular responses to IFN-I.

Introduction

Human type I IFNs (IFN-Is) form a group of 19 potent antiviral and proinflammatory cytokines (Borden et al., 2007). IFN-Is are produced by almost any cell type in response to stimuli, particularly viral intermediates and byproducts (Kawai and Akira, 2008). Once induced, IFN-Is are secreted, and, in an autocrine and paracrine fashion, signal through the IFN-I receptor (IFNAR), which consists of two subunits, IFN-I receptor I (IFNAR1) and IFN-I receptor II (IFNAR2). Most, if not all, cells express the IFN receptor. Upon ligand binding, the IFN-I-IFNAR complex then initiates a signaling cascade via auto- and transphosphorylation of *JAK1* and *TYK2*, kinases that subsequently phosphorylate *STAT1* and *STAT2*. In complex with *IRF9*, *STAT1* and *STAT2* form the IFN-stimulated gene factor 3 (*ISGF3*) complex that translocates to the nucleus and initiates transcription of hundreds of IFN-I-stimulated genes (*ISGs*; Schindler et al., 2007; Stark and Darnell, 2012). Two *ISGs*, *ISG15* (Zhang et al., 2015)

and *USP18* (François-Newton et al., 2011; Meuwissen et al., 2016), form a complex that negatively regulates the response to IFN-I. Namely, *USP18*, which when bound by *ISG15* is more stable, displaces *JAK1* (François-Newton et al., 2012) from *IFNAR2*, thereby terminating responses to IFN-I.

Both loss and gain of IFN-I activity have dire consequences for humans (Taft and Bogunovic, 2018). Patients with autosomal recessive *IFNAR1* (Hernandez et al., 2019), *IFNAR2* (Duncan et al., 2015), *TYK2* (Kreins et al., 2015), *STAT1* (Dupuis et al., 2003), *STAT2* (Hambleton et al., 2013), and *IRF9* (Hernandez et al., 2018) deficiencies all suffer from severe viral diseases. In contrast, type I interferonopathies are monogenic disorders that result from autoinflammation caused by excessive IFN-I activity (Rodero and Crow, 2016). The concept was established and the term coined by Yanick Crow (Crow, 2011; Rodero and Crow, 2016). Known etiologies disrupt either of two distinct cellular

¹Department of Microbiology, Icahn School of Medicine at Mt. Sinai, New York, NY; ²Laboratory of Clinical Immunology, Inflammation and Allergy, Faculty of Medicine and Pharmacy of Casablanca, King Hassan II University, Casablanca, Morocco; ³Clinical Immunology Unit, Department of Pediatric Infectious Diseases, Children's Hospital, Centre Hospitalier Universitaire Averroes, Casablanca, Morocco; ⁴Paris University, Imagine Institute, Paris, France; ⁵Laboratory of Human Genetics of Infectious Diseases, Institut National de la Santé et de la Recherche Médicale U1163, Necker Hospital for Sick Children, Paris, France; ⁶St. Giles Laboratory of Human Genetics of Infectious Diseases, Rockefeller Branch, The Rockefeller University, New York, NY; ⁷Howard Hughes Medical Institute, New York, NY; ⁸Pediatric Hematology and Immunology Unit, Necker Hospital for Sick Children, Assistance Publique-Hôpitaux de Paris, Paris, France; ⁹Center for the Study of Primary Immunodeficiencies, Necker Hospital for Sick Children, Assistance Publique-Hôpitaux de Paris, Paris, France; ¹⁰Department of Pediatrics, Icahn School of Medicine at Mt. Sinai, New York, NY; ¹¹Precision Immunology Institute, Icahn School of Medicine at Mt. Sinai, New York, NY; ¹²Mindich Child Health and Development Institute, Icahn School of Medicine at Mt. Sinai, New York, NY.

Correspondence to Dusan Bogunovic: dusan.bogunovic@mssm.edu.

© 2020 Gruber et al. This article is distributed under the terms of an Attribution-Noncommercial-Share Alike-No Mirror Sites license for the first six months after the publication date (see <http://www.rupress.org/terms/>). After six months it is available under a Creative Commons License (Attribution-Noncommercial-Share Alike 4.0 International license, as described at <https://creativecommons.org/licenses/by-nc-sa/4.0/>).

mechanisms. The production of IFN-I can be excessive, owing to biallelic loss-of-function (LOF) mutations in self-RNA and DNA digesting enzymes or monoallelic gain-of-function (GOF) mutations in RNA and DNA cytoplasmic sensors (Rodero and Crow, 2016). Alternatively, there can be hyperactive responses to IFN-I by biallelic LOF mutations in negative regulators of IFN-I, such as *ISG15* (Zhang et al., 2015) and *USP18* (Meuwissen et al., 2016), or by heterozygous GOF mutations in *JAK1* (Del Bel et al., 2017; Gruber et al., 2019 Preprint) and *STAT1* (Liu et al., 2011). Herein, we studied a child who died of unexplained, severe, early-onset type I interferonopathy.

Results and discussion

Ex vivo phenotyping reveals type I interferonopathy

We studied a patient (P1; II.9) born to consanguineous patients from Morocco who presented with an early-onset, severe autoinflammation evocative of type I interferonopathy. He presented with skin ulcerations, seizures, cerebral calcifications, and ultimately respiratory failure and death (see Materials and methods for clinical details; Fig. 1 A). Of note, two siblings had previously died from complications that appeared infectious in origin but without an identified pathogen. We first measured whole-blood mRNA levels of four ISGs, including *IFIT1*, *IFI27*, *RSAD2*, and *ISG15*, all of which were elevated nearly 1,000-fold in the patient as compared with healthy donors or the heterozygous mother (Fig. 1 B). Furthermore, using SiMoA, a digital ELISA that allows for attomolar sensitivity in IFN- α detection, we detected drastically high levels of IFN- α in patient plasma (1,000 fg/ml as compared with an average 50 fg/ml in healthy controls; Fig. 1 C). Given these classical features of type I interferonopathy in immune peripheral cells (Rodero and Crow, 2016), we then examined the composition of peripheral blood mononuclear cells (PBMCs). We detected a distribution of immune cell types that was largely consistent with infancy, but with low frequencies of natural killer (NK) cells and monocytes and elevations in T cells, suggesting a dysregulated immunophenotype (Fig. 1, D and E; and Table S1, Table S2, and Table S3). Given the overt IFN-I signature, we analyzed surface expression of SIGLEC1 (CD169), an ISG, and determined that myeloid cells (classical monocytes in particular; CD14⁺CD16^{low}) and dendritic cells had significantly augmented expression of CD169 (Fig. 1 F). Combined, these ex vivo analyses confirmed bona fide type I interferonopathy.

Whole-exome sequencing (WES) reveals a homozygous mutation in *STAT2*

We performed WES of P1 and searched for candidate genetic variants, testing an autosomal recessive model, given the consanguinity and history of prior infant deaths in the family (Fig. 2 A). A homozygous variant was identified in exon 5 of the signal transducer and activator of transcription 2 (*STAT2*) at position c.443G>A, which results in the substitution of the arginine at position 148 by a glutamine, p.R148Q (Fig. 2, A and B). No other putative disease-causing alleles were detected in any of the 19 genes known to be responsible for interferonopathies (Rodero and Crow, 2016; Fig. S1 A). There were eight other homozygous

rare nonsynonymous variations, none of which were in a gene known to be related to IFN-I (Table S4). Sanger sequencing of exon 5 of *STAT2* confirmed the homozygous variant of genomic DNA from whole blood and fibroblasts from P1 (Fig. 2 C). DNA from the mother was heterozygous for this variant, while the father's DNA was unavailable. In silico analysis revealed that the variant was predicted to be protein damaging by combined annotation-dependent depletion (score = 24.1, above the mutation significance cutoff of 2.313; Fig. S1 B). The variant is located in the coiled-coil domain of *STAT2* at a residue (148) that is highly conserved across mammals, but not in rodents (Fig. 2 D). This variant is absent in our in-house database of >6,000 WES and in public databases (the Greater Middle East Variome or in the gnomAD v2.1). There are only eight nonsynonymous *STAT2* variations found in homozygosity in public databases, none of which are predicted to be LOF. The homozygous mutations in *STAT2* that were previously shown to be loss of expression and LOF in patients with severe viral disease were private (Hambleton et al., 2013; Moens et al., 2017). Altogether, these findings suggested that the c.443G>A allele may be disease causing. As patients homozygous for loss-of-expression *STAT2* mutations had impaired responses to IFN-I and viral diseases, our findings further suggested that P1 might be homozygous for a *STAT2* mutation that is GOF for ISGF3 activity or LOF for a function other than ISGF3 activity or both.

The R148Q *STAT2* variant is a GOF for late ISG induction

To characterize the allele in isolation of the patient's genetic background, we studied the patient's mutation in U6A cells, a fibrosarcoma human cell line that is *STAT2* null (Pellegrini et al., 1989). We transduced U6A cells with either *Luciferase* (negative control ["null"]), WT *STAT2*, or R148Q *STAT2*. We first detected that transduction with either WT or R148Q *STAT2* resulted in similar levels of *STAT2* mRNA and *STAT2* protein (Fig. 3 A and B). In addition, brief 4-h stimulation with IFN-I resulted in similar mRNA levels of *MXI* and *IFI27* (Fig. S2 A). In contrast, prolonged 16-h stimulation with IFN-I resulted in increased mRNA levels of *MXI*, *IFI27*, *IFIT1*, and *RSAD2* in U6A cells transduced with R148Q *STAT2* when compared with WT *STAT2* (Figs. 3 C and S2 C). Prolonged stimulation with IFN-II, which does not use *STAT2*, was normal (Fig. S2 B). We then hTERT-immortalized and tested dermal fibroblasts derived from the patient. Expression of *MXI*, *RSAD2*, *IFIT1*, and *IFI27* mRNA with prolonged IFN α 2b stimulation was significantly elevated in patient hTERT fibroblasts when compared with cells from healthy controls (Figs. 3 D and S2 D). We then tested whether this phenotype requires homozygosity. We coexpressed WT and R148Q *STAT2* in U6A cells. In this system, upon IFN-I stimulation, the presence of WT *STAT2* rescued the heightened signaling afforded by R148Q *STAT2* (Fig. 3 E), whereas transduction with the negative control did not. Cells from heterozygous relatives of the patient were not available. They were, however, healthy and had no elevation of ISGs in peripheral blood (Fig. 1 B), suggesting that the GOF mutation likely has no impact in heterozygosity. Collectively, these experiments indicate that the *STAT2* mutation is GOF in isolation and that the biallelic genotype also results in gain of ISGF3 activity at late time points.

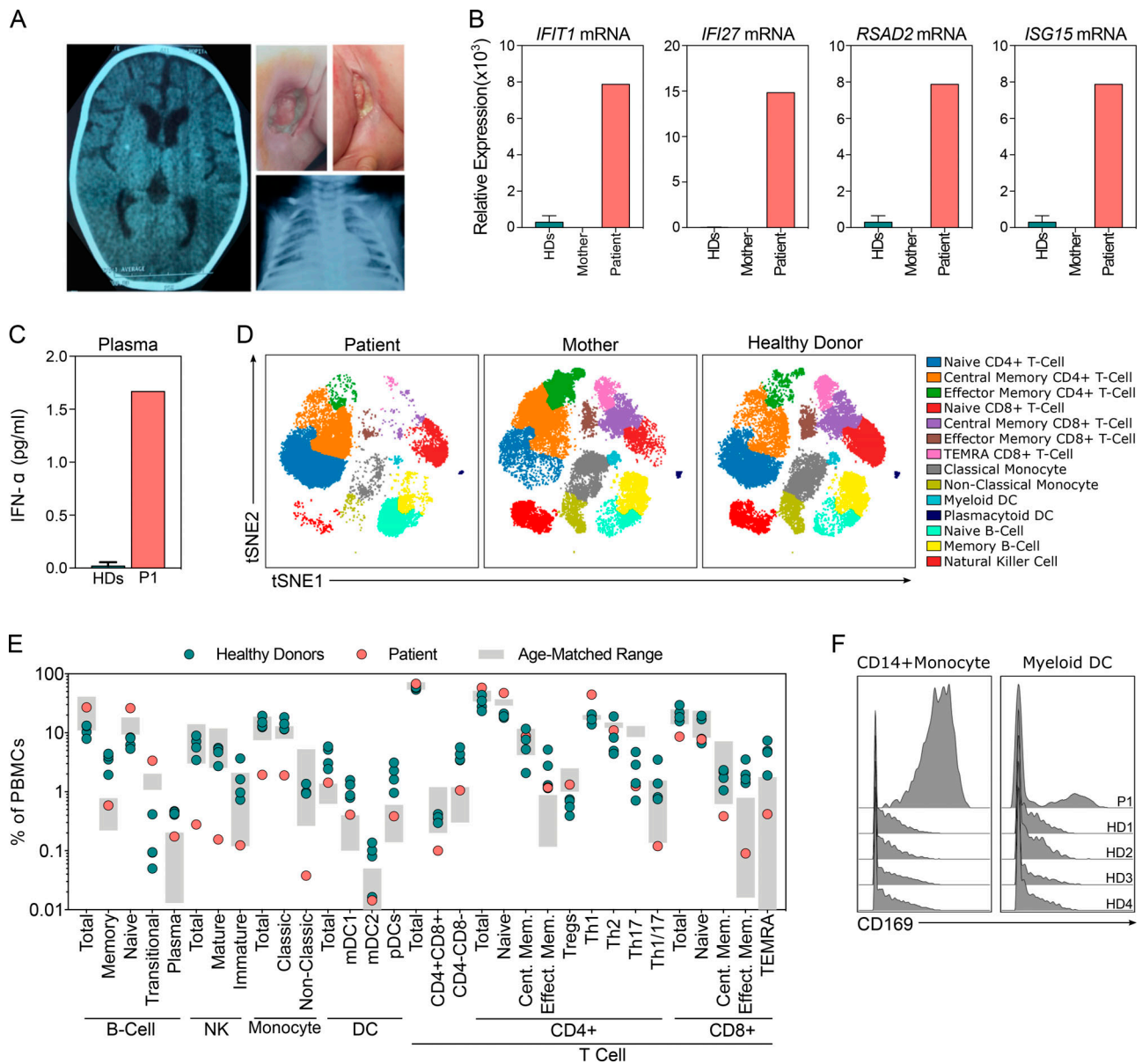


Figure 1. Peripheral blood signature indicates autosomal recessive type I interferonopathy. (A) Clinical signs of immune pathology, clockwise from top: CT scan demonstrating calcifications of the frontal and parietal lobes, fistulizing adenitis of the axillary and inguinal nodes, and chest radiograph displaying bilateral opacities of the lungs. (B) mRNA expression of IFN-stimulated genes measured from whole-blood RNA isolated from healthy donors (HDs; $n = 3$), the patient's mother, and the patient. Error bars represent one standard deviation. (C) Quantification of circulating IFN- α by digital ELISA (single-molecule array) in plasma from three healthy controls (HD) and the patient (P1). (D) t -Distributed stochastic neighbor embedding (tSNE) plots demonstrating the immunophenotype of PBMCs as determined by mass cytometry. (E) Quantification of immune cell populations of four healthy donors and the patient expressed as percent of total PBMCs, with age-matched healthy range in gray. (F) Histograms of CD169 expression, an IFN-stimulated gene, in classical monocytes and myeloid dendritic cells. (DC). Th, T helper cell. TEMRA, terminally differentiated effector memory cells re-expressing CD45RA.

Loss of STAT2-mediated recruitment of USP18 results in GOF signaling in R148Q STAT2

Two functions of STAT2 are known. As part of the ISGF3 transcription factor complex, STAT2 is essential for cellular responses to IFN-I and IFN-III downstream of their respective receptors. STAT2 was also recently discovered to shuttle USP18 to IFNAR2, where USP18 exerts its negative regulatory function of IFN-I responses (Arimoto et al., 2017). STAT2 is therefore a positive regulator of IFN-I, while it also contributes to the negative regulation of IFN-I once USP18 is produced. Given that

R148Q is located within the STAT2/USP18 interacting domain (Arimoto et al., 2017), we hypothesized that it retains positive ISGF3 activity but loses negative USP18-related regulatory function. We first tested proximal signaling in healthy control and patient hTERT fibroblasts by stimulating cells with a 15-min pulse of IFN α 2b. Both STAT1 and STAT2 phosphorylation were normal (Fig. 4 A), which was also the case in U6A cells (Fig. S3, A and B). Nuclear localization after stimulation (Fig. 4, B and C) and subsequent nuclear export (Fig. S3 C) were also normal for the mutant STAT2. We then tested STAT2 dephosphorylation in

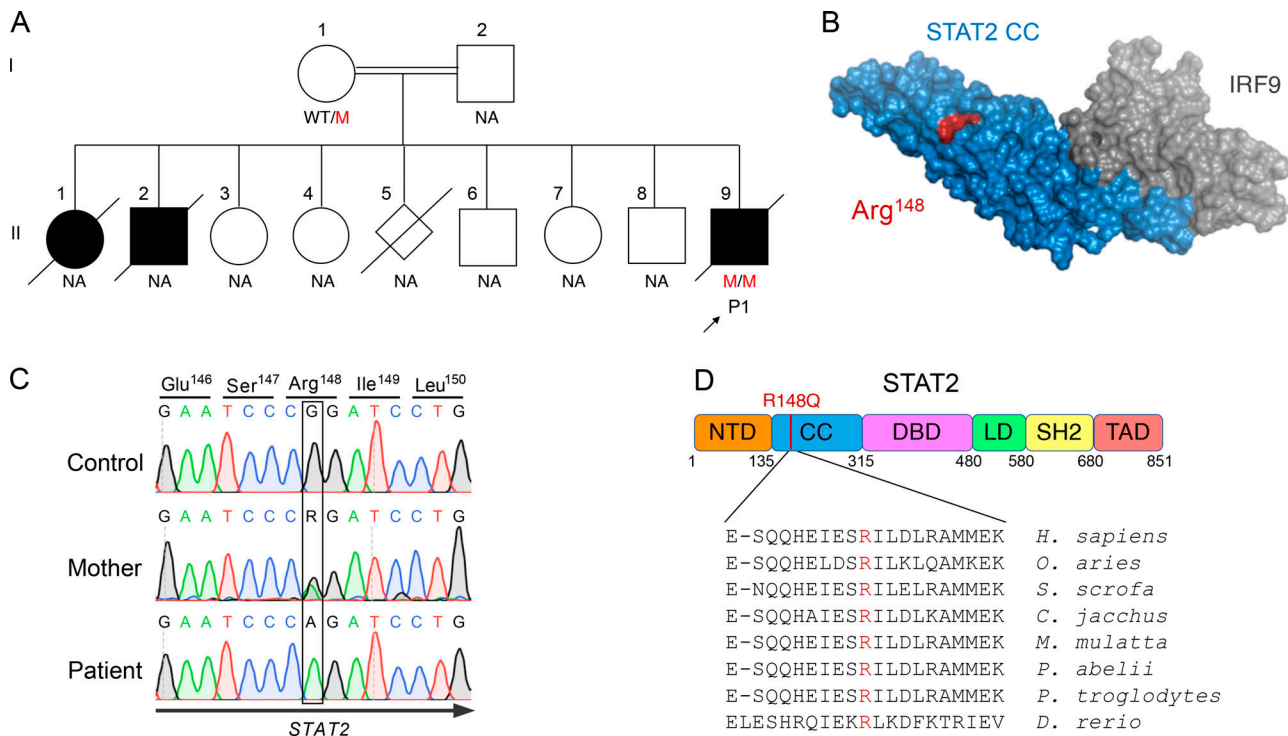


Figure 2. **Homozygous mutation affecting the coiled-coil domain of STAT2 identified in a patient with lethal autoinflammation.** (A) Family pedigree displaying affected individuals (shaded) and genotypes at position c.443 in STAT2. M indicates the STAT2 mutation and NA indicates individuals for whom the genotype was not available. (B) Crystal structure of murine STAT2 (blue) in complex with IRF9 (gray), demonstrating position of R148Q (red) in the coiled-coil domain, but outside of the STAT2/IRF9 interface. (C) Sanger sequencing of genomic DNA from the patient, his mother, and a healthy donor. (D) Schematic of STAT2 structure, indicating localization of the mutated residue and its conservation across mammals. CC, coiled-coil domain; DBD, DNA-binding domain; LD, linker domain; NTD, N-terminal domain; SH2, Src homology domains; TAD, transactivation domain.

the immediate hours after IFN-I exposure, which appeared equal between WT and patient cells (Fig. 4 D). We also determined the ability of WT and R148Q STAT2 to immunoprecipitate with USP18. The mutant protein exhibited similar affinity toward USP18, indicating that interaction was still possible, although function was likely perturbed (Fig. 4 E). We then evaluated USP18 localization to IFNAR2 in the presence of WT or R148Q STAT2. By immunoprecipitation of the receptor complex, we detected a reduced ability of R148Q STAT2 to recruit USP18 to IFNAR2 (Fig. 4, F and G). To functionally access this improper STAT2-USP18 homing, we tested the negative regulatory function of USP18/STAT2 R148Q by its capacity to prevent continual signaling. In cells WT for STAT2, stimulation with IFN-I leads to induction of USP18, which then significantly attenuates secondary challenge with IFN-I. While this was indeed the case in WT hTERT fibroblasts, patient fibroblasts were unable to attenuate proximal signaling upon IFN-I restimulation, despite accumulating levels of USP18 (Fig. 4 H). This effect was also observed in the U6A system (Fig. S3 D) and is akin to the response in complete USP18 deficiency (Fig. S3 E). To demonstrate that this late defect results specifically from a failure of USP18 function, we overexpressed USP18 in cells carrying WT STAT2 or STAT2 R148Q. While cells carrying WT STAT2 with USP18 were largely refractory to IFN-I stimulation, USP18 was functionally null in cells with STAT2 R148Q (Fig. 4 I). Collectively, these results suggest a defect in trafficking of USP18 to the

receptor and explain both the GOF and recessive inheritance of STAT2 R148Q (diagrammed in Fig. 4 J).

In the IFN-I signaling cascade, a homozygous GOF variant has never been reported until this discovery. To our knowledge, there are only two other documented strictly homozygous GOF mutations described in human genetics, one in hypocalcemic hypoparathyroidism caused by homozygous mutations in CASR (Cavaco et al., 2018) and another more recently in recurrent respiratory papillomatosis caused by homozygous mutations in NLRP1 (Drutman et al., 2019). Perhaps the MEFV mutations observed in familial Mediterranean fever may also be considered in this category, albeit with incompletely understood inheritance patterns and molecular mechanisms (Schnappauf et al., 2019). The existence of a homozygous GOF mutation in STAT2 is surprising given that STAT2 is predominantly considered a positive regulator of the IFN-I pathway by its essential role in the transcription factor complex. Remarkably, while this article was in review, Duncan et al. (2019) reported another homozygous STAT2 GOF mutation at the same residue (R148W) leading to a similar lethal phenotype. Molecularly, STAT2 R148Q associates with USP18 but fails to appropriately shuttle USP18 to IFNAR2, while STAT2 R148W was reported to associate poorly with USP18. Together, these reports substantiate the essential role for STAT2 to facilitate negative regulation (Arimoto et al., 2017). Thus, for homozygous GOF mutations in STAT2 to exist, mutations must affect USP18, but not intrinsic ISGF3, activity, as

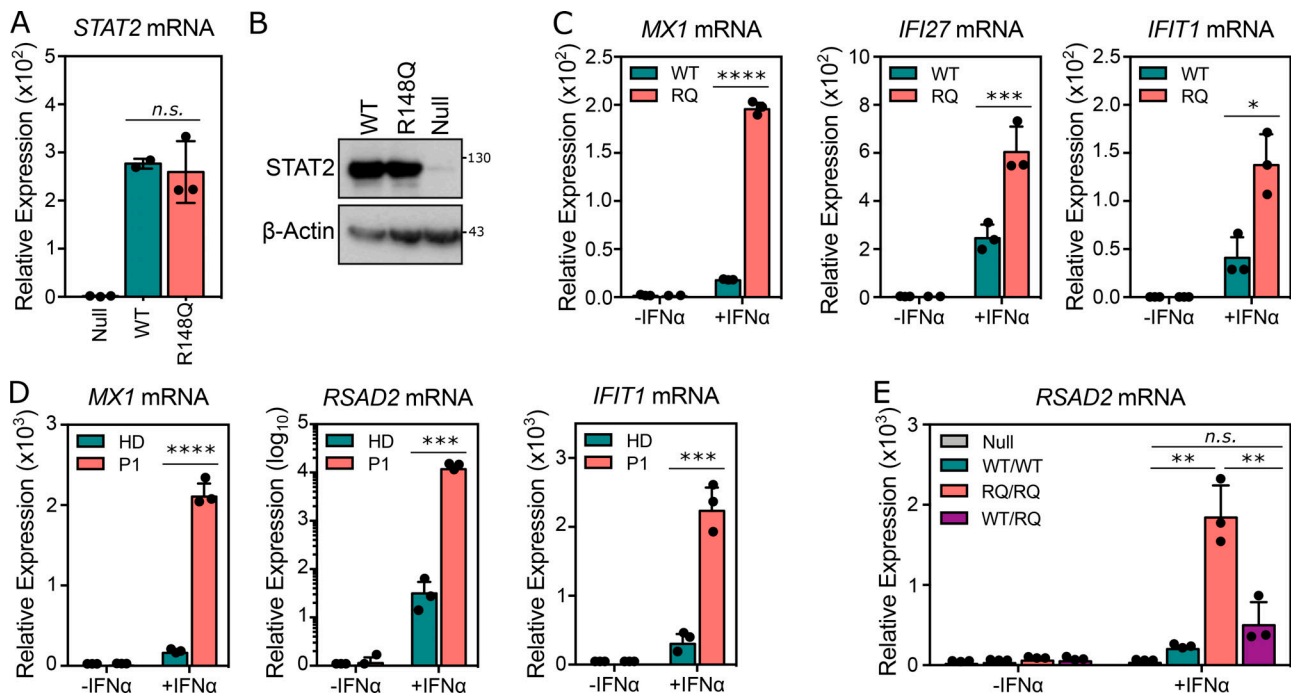


Figure 3. STAT2 R148Q leads to hyperinduction of ISGs, which can be rescued by WT STAT2. (A) STAT2 transcript levels in U6A cells (*STAT2*^{-/-}) reconstituted with an empty vector, WT STAT2 (WT), or R148Q STAT2 (RQ). Nonsignificant (n.s.) differences were determined by a P value > 0.05 from an unpaired two-tailed Student's *t* test. (B) STAT2 protein levels by Western blot in HEK293T cells transfected with indicated plasmids. (C) Expression of ISGs in transduced U6A cells after 16 h of 100 IU/ml IFN- α stimulation. Statistical testing by Student's *t* test. (D) Induction of ISGs in hTERT-immortalized fibroblasts. Statistical testing by Student's *t* test. (E) Transfection of WT STAT2 (WT; teal), R148Q STAT2 (RQ; salmon), or both (purple) in U6A cells, followed by overnight stimulation with IFN- α . Statistical analysis performed by one-way ANOVA. All results are representative of at least three independent experiments each with biological triplicates. Error bars represent one standard deviation. P values for all statistical testing correspond to *, *P* ≤ 0.05; **, *P* ≤ 0.01; ***, *P* ≤ 0.001; ****, *P* ≤ 0.0001.

documented in both STAT2 GOF mutations. For these reasons, homozygous GOF mutations may remain exquisitely rare, as the pathogenic mutations must perturb negatively regulatory domains while sparing principal functions.

The patient reported here suffered from severe early-onset inflammation characteristic of type I interferonopathies. STAT2 deficiency, alongside ISG15 and USP18 deficiencies, now constitutes a third genetic etiology leading to inadequate control of late cellular responses to IFN-I. Of note, this novel disease largely phenocopies USP18 deficiency in clinical presentation and molecular mechanism (Alsohime et al., 2020; Meuwissen et al., 2016). Clearly, tight control of IFNAR is essential for viability. If diagnosed and treated rapidly, as was the case in a recent USP18-deficient child, perhaps JAK inhibitor therapy would have rescued the life of this unfortunate child and his deceased siblings (Alsohime et al., 2020). This possibility is further substantiated by several recent studies that successfully introduced JAK inhibitors in a diverse range of genetic etiologies of type I interferonopathies (Sanchez et al., 2018). In the future, genetic diagnosis of rare STAT2 mutations, especially in the USP18 interacting domain, should alert clinicians toward fast therapeutic interventions with current and new classes of JAK inhibitors, as they can indeed be lifesaving.

Materials and methods

Genomic DNA extraction and WES

Genomic DNA was isolated from the whole blood of the patient, his mother, and healthy donors with iPrep instruments from

Thermo Fisher Scientific. 3 μ g of DNA was used for generation of WES from P1. The Agilent 50 Mb SureSelect exome kit was used in accordance with the manufacturer's instructions. BWA aligner was used to align the reads with the human reference genome hg19, before recalibration and annotation with GATK, PICARD, and ANNOVAR. Filter of variants was achieved with our in-house software. Mutation was verified by Sanger methods (PCR amplification conditions are available upon request). PCR products were analyzed by electrophoresis in 1% agarose gels, sequenced with the V3.1 Big Dye terminator cycle sequencing kit, and analyzed on an ABI Prism 3700 machine (Applied Biosystems).

Cell culture

HEK293T, U6A, and hTERT-immortalized dermal fibroblasts from the patient were cultured in DMEM (Gibco) supplemented with 10% FBS (Invitrogen), GlutaMAX (350 ng/ml; Gibco), and penicillin/streptomycin (Gibco). All cells were cultured at 37°C and 10% CO₂. All cell lines were tested for mycoplasma contamination with the MycoAlert PLUS Mycoplasma Detection Kit (Lonza) according to the manufacturer's instructions. U6A cells (*STAT2*^{-/-}) were a gift from Dr. Sandra Pellegrini (Institut Pasteur, Paris, France).

RNA isolation and quantitative PCR

All cytokine stimulations were performed as indicated with IFN- α 2b (Intron-A) or IFN- γ (570202; BioLegend) in complete

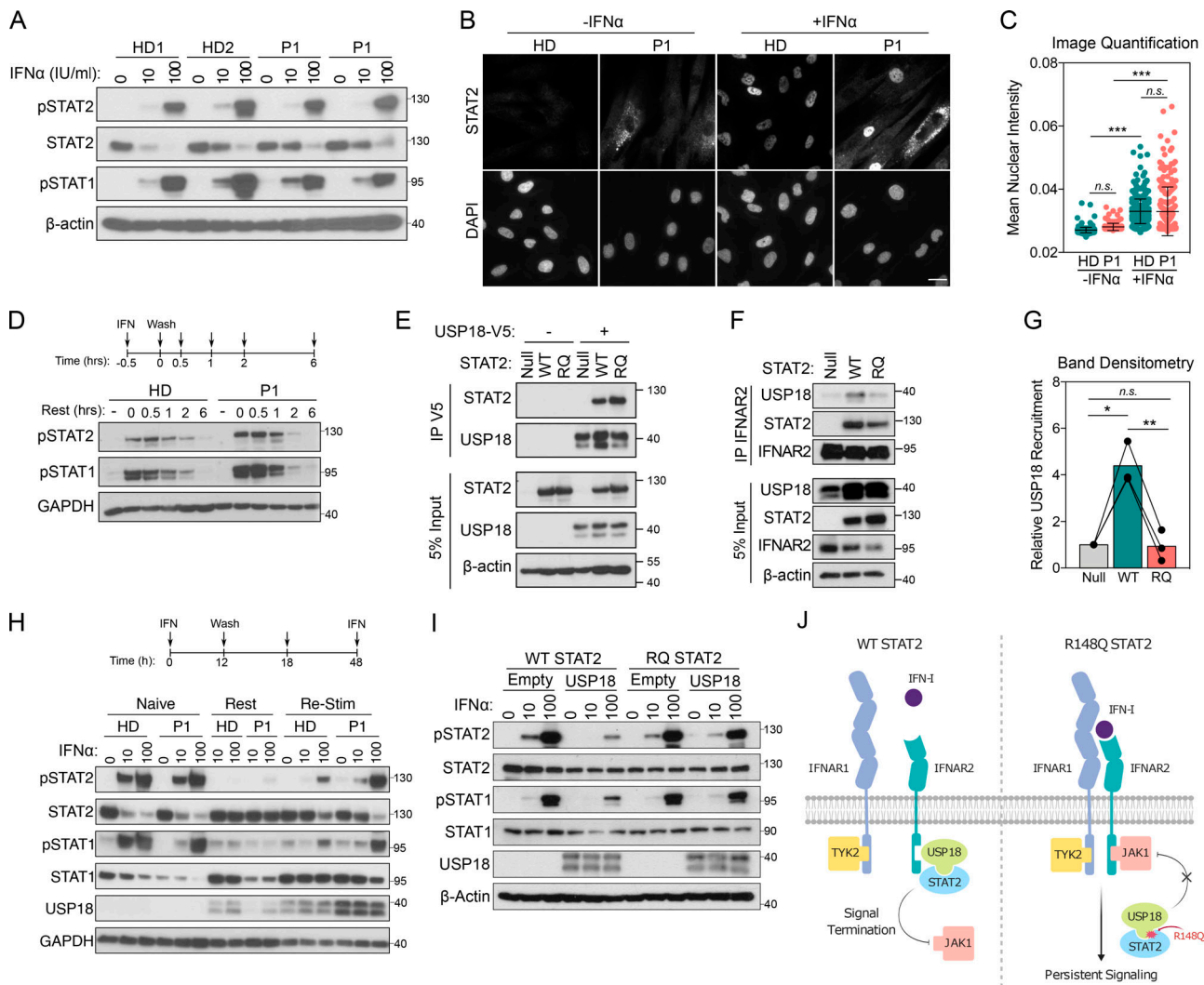


Figure 4. Intact proximal, but not late, signaling with STAT2 R148Q owing to defective USP18-mediated negative regulation. (A) Analysis of STAT1 and STAT2 phosphorylation in dermal fibroblasts following 15-min stimulation with indicated doses (IU/ml) of IFN- α . Separate healthy donors (HD1 and HD2) and two biological replicates of patient fibroblasts were tested. **(B)** Immunofluorescence staining of STAT2 translocation in fibroblasts after 30-min stimulation with 1,000 IU/ml IFN- α . Scale bar represents 25 μ m. **(C)** Nuclear translocation quantified in right panel. Statistical testing performed by one-way ANOVA, with n.s. indicating P values > 0.05. **(D)** Dephosphorylation of STAT1 and STAT2 in hTERT fibroblasts pulsed with IFN- α for 15 min, washed, and allowed to rest. **(E)** Transfection of indicated plasmids into HEK293T cells and subsequent immunoprecipitation (IP) of USP18-V5 to measure interaction with STAT2. **(F)** Recruitment of USP18 to the receptor in U6A cells transduced with negative control, WT STAT2, or mutant STAT2 and transfected with IFNAR2-Flag and USP18-V5. Immunoprecipitation performed against IFNAR2-Flag. **(G)** Band densitometry of relative USP18 quantities coimmunoprecipitated with IFNAR2 in three independent experiments. Statistical testing by repeated-measures ANOVA. **(H)** Analysis of negative regulatory capability by stimulating cells which had previously been stimulated (restim) or not (naive) with a primary stimulus of IFN- α for 12 h, washed, and allowed to rest for 6 h (rest) or 36 h before a restimulation with indicated doses of IFN- α . **(I)** IFN stimulation in U6A cells carrying WT STAT2 or R148Q STAT2 transduced with USP18 or without (empty). Stimulations were performed with indicated doses of IFN- α for 15 min. **(J)** Schematic demonstrating USP18 action in cells carrying WT STAT2 versus R148Q STAT2. All results are representative of three independent experiments. Error bars represent one standard deviation. P values for all statistical testing correspond to *, P \leq 0.05; **, P \leq 0.01; ***, P \leq 0.001.

DMEM. RNA was extracted from U6A cells, hTERT-immortalized fibroblasts (Qiagen RNeasy) or whole blood (PAXgene Blood RNA Kit) and reverse-transcribed (ABI High Capacity Reverse Transcription). The expression of ISGs (*IFIT1*, *MX1*, *RSAD2*, *IFI27*, and *ISG15*), relative to the 18S housekeeper gene, was analyzed by TaqMan quantitative real-time PCR (TaqMan Universal Master Mix II with uracil-DNA glycosylases) on a Roche LightCycler 480 II. The relative levels of ISG expression were calculated by the $\Delta\Delta$ CT method, relative to the mean values for the mock-treated controls or healthy donor.

Ectopic expression

HEK293T cells were transiently transfected with Lipofectamine 2000 (Thermo Fisher Scientific) complexed with different constructs according to manufacturer’s instructions. The following gene constructs were used for expression and coimmunoprecipitation: pTRIP-USP18-V5, PLX304-IFNAR2, and pTRIP-STAT2 (WT and R148Q). R148Q mutation was generated by site-directed mutagenesis on a WT STAT2 plasmid using QuickChange II PCR (Agilent). Lentiviral particles were generated by cotransfection of STAT2, psPAX2, and pMD2 by CaCl₂ transfection. Supernatants

were collected 48 h later, purified, and transferred to target cells with polybrene. Cells were selected with puromycin (0.4 $\mu\text{g}/\text{ml}$). To compensate for equivalent levels of ectopic expression, transfection and transduction experiments were matched with an irrelevant gene (*Luciferase*) in the same plasmid construct.

Protein assays

Whole-cell extracts for immunoblotting were prepared by incubating cells for 10 min in RIPA lysis buffer (Thermo Fisher Scientific) with 50 mM dithiothreitol and Protease/Phosphatase inhibitor cocktail (Cell Signaling Technology). For coimmunoprecipitation assay, cells were lysed in 50 mM Tris, pH 6.8, 0.5% NP-40, 200 mM NaCl, 10% glycerol, 1 mM EDTA, and 1 \times Protease/Phosphatase inhibitor cocktail (Cell Signaling Technology). Cell lysates were incubated with V5 conjugated with protein G dynabeads for 2 h at room temperature. Immunoprecipitates were subjected to Western blotting. Immunoblotting was performed using the Bio-Rad Western blot workflow. Membranes were blocked in 5% BSA for primary antibodies or 5% nonfat dry milk for secondary antibodies. Antibodies used were STAT1 (Santa Cruz Biotechnology), STAT2 (Millipore), phospho-Tyr 701 STAT1 (Cell Signaling Technology), phospho-Tyr 689 STAT2 (Millipore), USP18 (Cell Signaling Technology), β -actin (ABclonal), and GAPDH (Millipore). Signal was detected with enhanced chemiluminescence detection reagent (SuperSignal West pico; Thermo Fisher Scientific) by film development.

Mass cytometry

Whole blood from the patient and healthy controls were subject to Ficoll gradient to collect the mononuclear cell layer (PBMC). PBMCs were stained and analyzed by mass cytometry (CyTOF) at the Human Immune Monitoring Center of the Icahn School of Medicine at Mt. Sinai. Samples were barcoded then stained together with antibodies against selected surface markers for 30 min on ice. Cells were then washed and fixed, resuspended in dH_2O containing EQ Four Element Calibration Beads (Fluidigm), and acquired on a CyTOF2 Mass Cytometer (Fluidigm). Data files were normalized by using a bead-based normalization algorithm (CyTOF software, Fluidigm) and debarcoded using CD45 gating. The gated populations were visualized in lower dimensions using viSNE in Cytobank (<https://www.cytobank.org/>) and manually gated based on the following traditionally defined markers: CD45-Y89, CD57-In113, CD11c0In115, CD33-Pr141, CD19-Nd142, CD45RA-Nd143, CD141-Nd144, CD4-Nd145, CD8-Nd146, CD20-Sm147, CD16-Nd148, CD127-Sm149, CD1c-Nd150, CD123-Eu151, CD66b-Sm152, PD1-Eu153, CD86-Sm154, CD27-Gd155, CCR5-Gd16, CD117-Gd158, CD25-Tb159, CD15-Gd160, CD56-Dy161, CD169-Dy162, CRTH2-Dy163, CD371-Dy164, CCR6-Ho165, CD25-Er166, CCR7-Er167, CD3-Er168, CX3CR1-Tm168, CD38-Er170, CD161-Yb171, CD209-Yb172, CXCR3-Yb173, HLADR-Yb174, CCR4-Yb176, and CD11b-Bi209.

Immunohistochemistry

Fibroblasts were seeded in 8-well chamber slides (80826; Ibidi) and stimulated the following day with 1,000 U/ml IFN- α for 30 min or 12 h. The cells were fixed and permeabilized (554714; BD) and then stained with DAPI and antibodies against STAT2

(EMD 06-502, 1:200). The samples were evaluated on the Leica DMI8.

Flow cytometry

Transduced U6A cells were stimulated for 15 min with IFN α 2b and then immediately fixed with 4% PFA for 10 min. Cells were then fixed/permeabilized in 90% ice-cold methanol and stained with anti-phospho-STAT1 (9167; Cell Signaling Technology), a fluorescent secondary antibody (Thermo Fisher Scientific) and a LIVE/DEAD viability dye (Thermo Fisher Scientific). Flow cytometry was acquired on a BDFACSCanto II, and data were analyzed with FlowJo.

SiMoA digital ELISA

Plasma samples from the patient and healthy donors were isolated by Ficoll gradient and subsequently clarified by centrifugation at high speeds. IFN- α levels were then quantified by digital ELISA using the IFN α SiMoA Assay Kit (100860; Quanterix) according to the manufacturer's instructions on a SiMoA HD1 Analyzer.

Case report

We investigated one patient from a consanguineous family (second degree) from Morocco (Figs. 1 A and 2 A). P1 (II.9) was a boy born in November 2015 at 38 wk of gestation, without any problems during the pregnancy. At birth, he received the bacillus Calmette-Guérin vaccine, without secondary effects. At the age of 15 d, he presented with diarrhea, oral thrush, and axillar and inguinal adenitis. At the age of 22 d, he was hospitalized due the fistulation of adenitis (Fig. 2 A); cultures of samples were positive for *Klebsiella pneumoniae* extended-spectrum B lactamase enzymes and *Pseudomonas aeruginosa*; direct staining for acid fast bacilli was negative (Fig. 1 A). Histology revealed reactive lymphoid hyperplasia. He received treatment with gentamicin and ceftriaxone, but this was rapidly replaced by amikacin, ceftazidime, and imipenem, resulting in clinical improvement. However, during this hospitalization, he had two other findings marked by bronchiolitis and seizures unrelated to the fever (Fig. 2 A). Cerebral computed tomography (CT) revealed brain bilateral calcifications distributed in the frontal and parietal regions (Fig. 2 A). Laboratory tests revealed anemia and mild leukocytosis. Levels of IgG, IgM, and IgA were within the age-matched reference range. Immunophenotyping of T, B, and NK cells, as well as a dihydrorhodamine 123 assay on neutrophils, were normal at that time (Table S2). He was assumed to have an inborn error of immunity. At the age of 5 mo, he was hospitalized for respiratory manifestations of disease. Chest radiographs revealed cardiomegaly, bilateral opacities of the lungs with an interstitial pattern, and absence of pleural effusion. Chest CT scan was suggestive of pulmonary alveolar proteinosis, but bronchoalveolar lavage fluid testing was not performed. Results of PCR for cytomegalovirus were negative. Culture of blood was negative for pyogenic bacteria, mycobacteria, and fungi. However, he received multiple antiviral and antifungal drugs, antibiotics (including those for mycobacterial infections), and steroids. He died during this hospitalization due to the aggravation of pulmonary disease leading to respiratory

insufficiency. The family had previously lost two infant siblings, a girl born in 1991 and a boy born in 1992. Both infants had fistulizing adenitis, and they died from disease that appeared infectious in origin but suggestive of uncontrolled inflammation. Other siblings (born in 1994, 1996, 2002, 2005, and 2008) are healthy and have never been referred for severe infectious diseases or seizures. All individuals received the bacillus Calmette–Guérin vaccine at the birth according to the Moroccan calendar of vaccines, and none had adverse effects.

The patient was referred to the Laboratory of Human Genetics of Infectious Disease, France, for genetic study. Parents signed an informed consent form, in accordance with the requirements of the institutional review boards of the various institutions involved. Approval for this study was obtained from the French Ethics Committee (Comité de Protection de Personnes), the French National Institute of Health and Medical Research (Institut National de la Santé et de la Recherche Médicale; 2010-A00650-39), and The Rockefeller University (JCA-0699).

Online supplemental material

Fig. S1 shows genetic analysis of a patient with early-onset type I interferonopathy. **Fig. S2** shows that STAT2 R148Q heightens target gene induction after stimulation with type I, but not type II, IFN. **Fig. S3** shows that STAT2 R148Q exhibits normal ISGF3 activity but fails to facilitate appropriate negative regulation. Table S1 lists patient immunological phenotype from the analysis of whole-blood samples. Table S2 lists immunoglobulin levels. Table S3 shows a tabulation of PBMC immune subset frequencies by CyTOF. Table S4 lists variants identified after analysis of the WES of the patient.

Acknowledgments

We thank Adeeb Rahman, Brian Lee, and Kevin Tuballes from Human Immune Monitoring Center at the Icahn School of Medicine for their technical assistance and guidance in experimental design. We would also like to thank Ludovic Debure and Dr. Thomas Wisniewski (recipient of grants AG08051 and R01AF058267) of the New York State Center of Excellence for Alzheimer’s Disease for their technical assistance with the SiMoA assay.

This research was supported by National Institute of Allergy and Infectious Diseases grants R01AI127372, R21AI134366, and R21AI129827 and by the March of Dimes (awarded to D. Bogunovic). C. Gruber was supported by T32 training grant 5T32HD075735-07 at the Icahn School of Medicine at Mount Sinai. J. Rosain is supported by Poste d’accueil INSERM. J. Taft is supported by the F31 training grant 5F31AI138363 at the Icahn School of Medicine at Mount Sinai. The Laboratory of Human Genetics of Infectious Diseases is supported by grants from the St. Giles Foundation, the Jeffrey Model Foundation, The Rockefeller University Center for Clinical and Translational Science (National Center for Research Resources and National Center for Advancing Translational Sciences grant 8UL1TR000043), National Institutes of Health (National Institute of Allergy and Infectious Diseases grants 5R01AI089970-02 and 5R37AI095983), the Integrative Biology of Emerging Infectious Diseases Laboratory of

Excellence (grant ANR-10-LABX-62-IBEID), Fondation pour la Recherche Médicale, and the French National Research Agency under the “Investments for the future” program (ANR-10-IAHU-01), GENMSMD (ANR-16-CE17-0005-01), Institut National de la Santé et de la Recherche Médicale, Paris Descartes University, and The Rockefeller University.

Author contributions: C. Gruber and M. Martin-Fernandez designed and performed most of the experiments, analyzed the data, and wrote the manuscript. J. Taft helped design and perform microscopy. X. Qiu performed immunoprecipitation experiments. S. Buta helped with cloning, tissue culture, and experiment execution. F. Ailal provided samples and performed clinical diagnoses and follow up of the kindred. A. Bousfiha, J. Rosain, J. Bustamante, and J.-L. Casanova provided patient samples, analyzed and/or interpreted data, and contributed to the writing of the paper. D. Bogunovic helped design the experiments and analyze data, supervised the work, and wrote the manuscript. All authors commented on the manuscript and approved its final version.

Disclosures: The authors declare no competing interests exist.

Submitted: 10 December 2019

Revised: 13 January 2020

Accepted: 7 February 2020

References

- Alsohime, F., M. Martin-Fernandez, M.H. Tamsah, M. Alabdulhafid, T. Le Voyer, M. Alghamdi, X. Qiu, N. Alotaibi, A. Alkahtani, S. Buta, et al. 2020. JAK Inhibitor Therapy in a Child with Inherited USP18 Deficiency. *N. Engl. J. Med.* 382:256–265. <https://doi.org/10.1056/NEJMoa1905633>
- Arimoto, K.I., S. Löchte, S.A. Stoner, C. Burkart, Y. Zhang, S. Miyauchi, S. Wilmes, J.B. Fan, J.J. Heinisch, Z. Li, et al. 2017. STAT2 is an essential adaptor in USP18-mediated suppression of type I interferon signaling. *Nat. Struct. Mol. Biol.* 24:279–289. <https://doi.org/10.1038/nsmb.3378>
- Borden, E.C., G.C. Sen, G. Uze, R.H. Silverman, R.M. Ransohoff, G.R. Foster, and G.R. Stark. 2007. Interferons at age 50: past, current and future impact on biomedicine. *Nat. Rev. Drug Discov.* 6:975–990. <https://doi.org/10.1038/nrd2422>
- Cavaco, B.M., L. Canaff, A. Nolin-Lapalme, M. Vieira, T.N. Silva, A. Saramago, R. Domingues, M.M. Rutter, J. Hudon, J.L. Gleason, et al. 2018. Homozygous Calcium-Sensing Receptor Polymorphism R544Q Presents as Hypocalcemic Hypoparathyroidism. *J. Clin. Endocrinol. Metab.* 103:2879–2888. <https://doi.org/10.1210/jc.2017-02407>
- Crow, Y.J. 2011. Type I interferonopathies: a novel set of inborn errors of immunity. *Ann. N. Y. Acad. Sci.* 1238:91–98. <https://doi.org/10.1111/j.1749-6632.2011.06220.x>
- Del Bel, K.L., R.J. Ragotte, A. Saferali, S. Lee, S.M. Vercauteren, S.A. Mostafavi, R.A. Schreiber, J.S. Prendiville, M.S. Phang, J. Halparin, et al. 2017. JAK1 gain-of-function causes an autosomal dominant immune dysregulatory and hypereosinophilic syndrome. *J. Allergy Clin. Immunol.* 139:2016–2020.e5. <https://doi.org/10.1016/j.jaci.2016.12.957>
- Drutman, S.B., F. Haerynck, F.L. Zhong, D. Hum, N.J. Hernandez, S. Belkaya, F. Rapaport, S.J. de Jong, D. Creytens, S.J. Tavernier, et al. 2019. Homozygous *NLRP1* gain-of-function mutation in siblings with a syndromic form of recurrent respiratory papillomatosis. *Proc. Natl. Acad. Sci. USA.* 116:19055–19063. <https://doi.org/10.1073/pnas.1906184116>
- Duncan, C.J., S.M. Mohamad, D.F. Young, A.J. Skelton, T.R. Leahy, D.C. Munday, K.M. Butler, S. Morfopoulou, J.R. Brown, M. Hubank, et al. 2015. Human IFNAR2 deficiency: Lessons for antiviral immunity. *Sci. Transl. Med.* 7:307ra154. <https://doi.org/10.1126/scitranslmed.aac4227>
- Duncan, C.J.A., B.J. Thompson, R. Chen, G.I. Rice, F. Gothe, D.F. Young, S.C. Lovell, V.G. Shuttleworth, V. Brocklebank, B. Corner, et al. 2019. Severe type I interferonopathy and unrestrained interferon signaling due to a

- homozygous germline mutation in *STAT2*. *Sci. Immunol.* 4:eav7501. <https://doi.org/10.1126/sciimmunol.aav7501>
- Dupuis, S., E. Jouanguy, S. Al-Hajjar, C. Fieschi, I.Z. Al-Mohsen, S. Al-Jumaah, K. Yang, A. Chapgier, C. Eidsenchen, P. Eid, et al. 2003. Impaired response to interferon-alpha/beta and lethal viral disease in human *STAT1* deficiency. *Nat. Genet.* 33:388–391. <https://doi.org/10.1038/ng1097>
- François-Newton, V., G. Magno de Freitas Almeida, B. Payelle-Brogard, D. Monneron, L. Pichard-Garcia, J. Piehler, S. Pellegrini, and G. Uzé. 2011. USP18-based negative feedback control is induced by type I and type III interferons and specifically inactivates interferon α response. *PLoS One.* 6:e22200. <https://doi.org/10.1371/journal.pone.0022200>
- Francois-Newton, V., M. Livingstone, B. Payelle-Brogard, G. Uzé, and S. Pellegrini. 2012. USP18 establishes the transcriptional and anti-proliferative interferon α/β differential. *Biochem. J.* 446:509–516. <https://doi.org/10.1042/BJ20120541>
- Gruber, C., J. Calis, S. Buta, G. Evrony, J. Martin, S. Uhl, R. Caron, L. Jarchin, D. Dunkin, R. Phelps, et al. 2019. Complex Autoinflammatory Syndrome Unveils Fundamental Principles of *JAK1* Transcriptional and Biochemical Function. *bioRxiv*. doi: 10.1101/807669 (Preprint posted October 17, 2019).
- Hambleton, S., S. Goodbourn, D.F. Young, P. Dickinson, S.M. Mohamad, M. Valappil, N. McGovern, A.J. Cant, S.J. Hackett, P. Ghazal, et al. 2013. *STAT2* deficiency and susceptibility to viral illness in humans. *Proc. Natl. Acad. Sci. USA.* 110:3053–3058. <https://doi.org/10.1073/pnas.1220098110>
- Hernandez, N., I. Melki, H. Jing, T. Habib, S.S.Y. Huang, J. Danielson, T. Kula, S. Drutman, S. Belkaya, V. Rattina, et al. 2018. Life-threatening influenza pneumonitis in a child with inherited *IRF9* deficiency. *J. Exp. Med.* 215:2567–2585. <https://doi.org/10.1084/jem.20180628>
- Hernandez, N., G. Buccioli, L. Moens, J. Le Pen, M. Shahrooei, E. Goudouris, A. Shirkani, M. Changi-Ashtiani, H. Rokni-Zadeh, E.H. Sayar, et al. 2019. Inherited *IFNAR1* deficiency in otherwise healthy patients with adverse reaction to measles and yellow fever live vaccines. *J. Exp. Med.* 216:2057–2070. <https://doi.org/10.1084/jem.20182295>
- Kawai, T., and S. Akira. 2008. Toll-like receptor and RIG-I-like receptor signaling. *Ann. N. Y. Acad. Sci.* 1143:1–20. <https://doi.org/10.1196/annals.1443.020>
- Kreins, A.Y., M.J. Ciancanelli, S. Okada, X.F. Kong, N. Ramírez-Alejo, S.S. Kilic, J. El Baghdadi, S. Nonoyama, S.A. Mahdavian, F. Ailal, et al. 2015. Human *TYK2* deficiency: Mycobacterial and viral infections without hyper-IgE syndrome. *J. Exp. Med.* 212:1641–1662. <https://doi.org/10.1084/jem.20140280>
- Liu, L., S. Okada, X.F. Kong, A.Y. Kreins, S. Cypowyj, A. Abhyankar, J. Toubiana, Y. Itan, M. Audry, P. Nitschke, et al. 2011. Gain-of-function human *STAT1* mutations impair IL-17 immunity and underlie chronic mucocutaneous candidiasis. *J. Exp. Med.* 208:1635–1648. <https://doi.org/10.1084/jem.20110958>
- Meuwissen, M.E., R. Schot, S. Buta, G. Oudesluijs, S. Tinschert, S.D. Speer, Z. Li, L. van Unen, D. Heijnsman, T. Goldmann, et al. 2016. Human *USP18* deficiency underlies type I interferonopathy leading to severe pseudo-TORCH syndrome. *J. Exp. Med.* 213:1163–1174. <https://doi.org/10.1084/jem.20151529>
- Moens, L., L. Van Eyck, D. Jochmans, T. Mitera, G. Frans, X. Bossuyt, P. Matthys, J. Neyts, M. Ciancanelli, S.Y. Zhang, et al. 2017. A novel kindred with inherited *STAT2* deficiency and severe viral illness. *J. Allergy Clin. Immunol.* 139:1995–1997.e9. <https://doi.org/10.1016/j.jaci.2016.10.033>
- Pellegrini, S., J. John, M. Shearer, I.M. Kerr, and G.R. Stark. 1989. Use of a selectable marker regulated by alpha interferon to obtain mutations in the signaling pathway. *Mol. Cell. Biol.* 9:4605–4612. <https://doi.org/10.1128/MCB.9.11.4605>
- Rodero, M.P., and Y.J. Crow. 2016. Type I interferon-mediated monogenic autoinflammation: The type I interferonopathies, a conceptual overview. *J. Exp. Med.* 213:2527–2538. <https://doi.org/10.1084/jem.20161596>
- Sanchez, G.A.M., A. Reinhardt, S. Ramsey, H. Wittkowski, P.J. Hashkes, Y. Berkun, S. Schalm, S. Murias, J.A. Dare, D. Brown, et al. 2018. *JAK1/2* inhibition with baricitinib in the treatment of autoinflammatory interferonopathies. *J. Clin. Invest.* 128:3041–3052. <https://doi.org/10.1172/JCI98814>
- Schindler, C., D.E. Levy, and T. Decker. 2007. *JAK-STAT* signaling: from interferons to cytokines. *J. Biol. Chem.* 282:20059–20063. <https://doi.org/10.1074/jbc.R700016200>
- Schnappauf, O., J.J. Chae, D.L. Kastner, and I. Aksentjevich. 2019. The Pyrin Inflammasome in Health and Disease. *Front. Immunol.* 10:1745. <https://doi.org/10.3389/fimmu.2019.01745>
- Stark, G.R., and J.E. Darnell Jr. 2012. The *JAK-STAT* pathway at twenty. *Immunity.* 36:503–514. <https://doi.org/10.1016/j.immuni.2012.03.013>
- Taft, J., and D. Bogunovic. 2018. The Goldilocks Zone of Type I IFNs: Lessons from Human Genetics. *J. Immunol.* 201:3479–3485. <https://doi.org/10.4049/jimmunol.1800764>
- Zhang, X., D. Bogunovic, B. Payelle-Brogard, V. Francois-Newton, S.D. Speer, C. Yuan, S. Volpi, Z. Li, O. Sanal, D. Mansouri, et al. 2015. Human intracellular *ISG15* prevents interferon- α/β over-amplification and auto-inflammation. *Nature.* 517:89–93. <https://doi.org/10.1038/nature13801>

Supplemental material

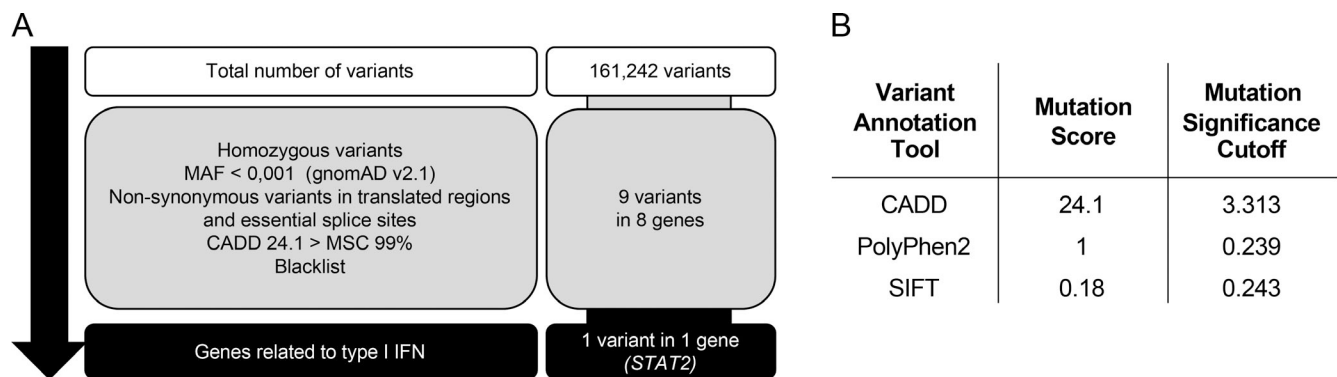


Figure S1. **Genetic analysis of a patient with early-onset type I interferonopathy. (A)** Schematic demonstrating variant analysis pipeline and results. **(B)** Prediction of functional impact of R148Q on STAT2 protein. CADD, combined annotation-dependent depletion. SIFT, sorting intolerant from tolerant.

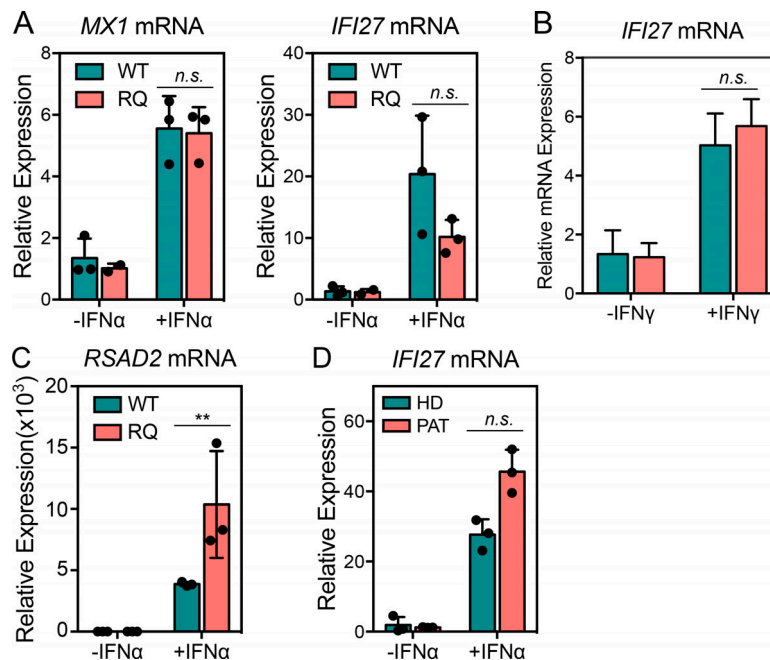


Figure S2. **STAT2 R148Q heightens target gene induction after stimulation with type I, but not type II, IFN. (A)** Stimulation of transduced U6A cells with IFN-I for 4 h. **(B)** Induction of target genes by IFN-II stimulation (5 ng/ml) for 16 h in transduced U6A cells. **(C)** Induction of *RSAD2* mRNA by IFN- α stimulation (100 IU/ml) for 16 h in transduced U6A cells. **(D)** Induction of *IFI27* mRNA by IFN- α stimulation (100 IU/ml) for 16 h in hTERT-immortalized cells. All experiments were performed on three occasions with biological triplicates. Error bars represent one standard deviation. P values for all statistical testing correspond to **, $P < 0.01$. n.s., not significant.

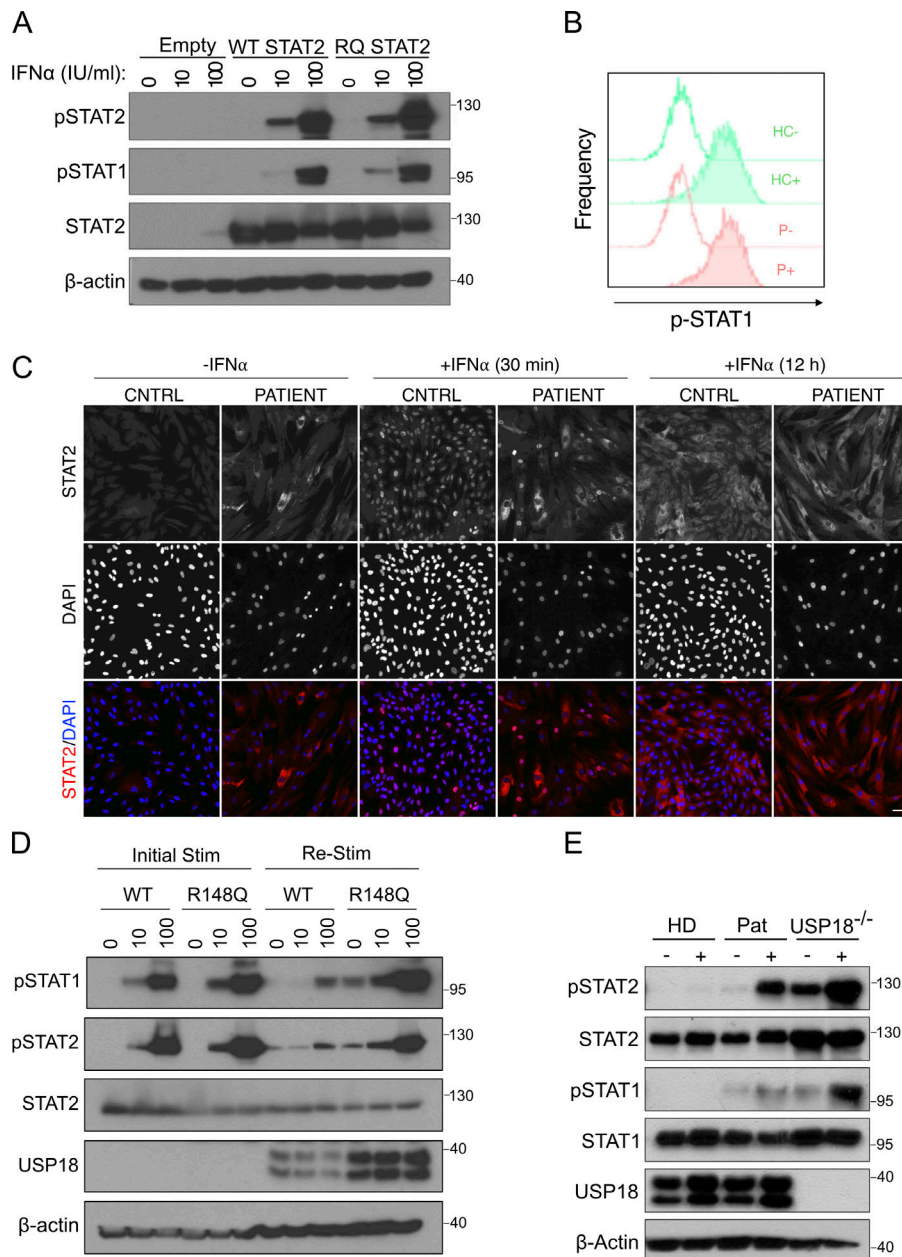


Figure S3. **STAT2 R148Q exhibits normal ISGF3 activity but fails to facilitate appropriate negative regulation.** (A) Analysis of STAT1 and STAT2 phosphorylation in transduced U6A cells following 15-min stimulation with indicated doses (IU/ml) of IFN- α . (B) Flow cytometry for STAT1 phosphorylation in U6As with WT (HC) or R148Q (P) STAT2, stimulated (+) or not (-) with IFN- α for 15 min. (C) Immunofluorescence staining of STAT2 translocation in fibroblasts after 30-min and 12-h stimulation with 1,000 IU/ml IFN- α . Scale bar represents 25 μ m. (D) Analysis of negative regulatory capability by stimulating cells that had previously been stimulated (restim) or not (naive) with a primary stimulus of IFN- α for 12 h, washed, and allowed to rest for 36 h before a restimulation with indicated doses of IFN- α . (E) IFN- α stimulation of healthy donor (HD), patient (Pat), or USP18-deficient fibroblasts that had previously been stimulated with IFN- α for 12 h and allowed to rest for 36 h. All results are representative of two or three independent experiments.

Tables S1–S4 are provided online as separate Word documents. Table S1 lists patient immunological phenotypes from the analysis of whole-blood samples. Table S2 lists immunoglobulin levels. Table S3 shows a tabulation of PBMC immune subset frequencies by CyTOF. Table S4 lists variants identified after analysis of the WES of the patient.